MRS Advances (2024) 9:373–380
https://doi.org/10.1557/s43580-024-00818-z

ORIGINAL PAPER

A structural-thermodynamic model of the $(U_{1-z}Pu_z)O_{2+\delta}$ solid solution

Victor L. Vinograd[1] · Andrey A. Bukaemskiy[1] · Guido Deissmann[1] · Giuseppe Modolo[1]

Received: 14 December 2023 / Accepted: 29 February 2024 / Published online: 22 March 2024

Abstract
Thermodynamic mixing properties of the $(U_{1-z}Pu_z)O_{2+\delta}$ fluorite solid solution are modelled by taking into account the dependence of the δ parameter on the chemical potential of O_2. Simultaneously, the model is made consistent with phase separation data that are relevant for the hypo-stoichiometric domain. An ion-packing approach is used to describe the variation in the lattice parameter as functions of z and δ. The linking of the ion-packing and thermodynamic models allows predicting the lattice parameter variation across the miscibility gap. The constructed diagrams provide means for estimating equilibration temperatures of biphasic assemblages from X-ray diffraction data.

Introduction

Uranium–plutonium-mixed oxides (MOX) are currently used as fuels in light water nuclear reactors and are discussed as prospective fuels for generation IV fast neutron reactors [1]. The knowledge of phase relations in the system of UO_2-$UO_{2.5}$-$PuO_{1.5}$-PuO_2 is important for various applications starting from an optimization of the synthesis of $(U,Pu)O_2$ solid solutions (incl. prospective MOX materials with elevated Pu content) and ending with the understanding of the thermodynamic stability of spent MOX fuels at interim storage and under long-term repository conditions. Experimental studies aimed at characterizing the chemical stability of spent MOX fuel at conditions relevant to deep geological repositories [2, 3] require samples characterized by specified composition and oxidation states and by a high degree of chemical homogeneity. Phase diagrams reveal, however, that hypo-stoichiometric $(U_{1-z}Pu_z)O_{2+\delta}$ solid solutions containing more than ~ 15 mol % of Pu oxide separate into high- and low-oxygen phases [4, 5]. The δ parameters of the high- and low-oxygen phases approach the limiting equations of $\delta = 0$ and $\delta = -z/2$, respectively, such that the gap widens at high Pu/(U + Pu) ratios. This heterogeneity could affect measured oxidative dissolution yields, e.g. by preventing an increase in the oxygen to metal (O/M) ratio above the value of 2.0 as long as the low-oxygen phase remains present. Consequently, it is important to detect the immiscibility and, when necessary, to modify synthesis or quenching routes such that the final state is represented by a single phase. Although the compositions of the exsolved phases can be accurately predicted as functions of the total composition and the temperature [6–8], none of the developed thermodynamic models provide equations allowing to directly compute the lattice parameters of the co-existing phases as functions of the thermodynamic parameters. On the other hand, the detection of the exsolution is most easily done with an in situ X-ray diffraction experiment. Here, we provide a solution to this problem by directly combining a thermodynamic model with a structural model. Importantly, the spectrum of experimental data, which could be used for parametrizing such a model, extends both into the thermodynamic and structural domains providing a higher level of confidence in its accuracy.

Methods

The thermodynamic model of the fluorite phase

The fluorite phase, $U_{1-z}Pu_zO_{2+\delta}$, is modelled as a mixture of the endmembers UO_2, $PuO_{1.5}$, PuO_2, $UO_{2.5}$ and $U_{0.5}Pu_{0.5}O_2$. The fifth endmember is built of equal amounts of Pu^{+3} and U^{+5} and is included following the results of a previous study [9] that suggested an importance of the $2U^{+4} = Ln^{+3} + U^{+5}$ substitution scheme. The Gibbs free

✉ Victor L. Vinograd
v.vinograd@fz-juelich.de

[1] Institute of Energy and Climate Research – Nuclear Waste Management (IEK-6), Forschungszentrum Jülich GmbH, Jülich, Germany

energies of the reduced endmembers UO_2 and $PuO_{1.5}$ are set to zero at all temperatures. The properties of the other endmembers are set equal to the Gibbs free energy effects of the chemical reactions

$$UO_2 = UO_{2.5} - \frac{1}{4}O_2 \tag{1}$$

$$PuO_{1.5} = PuO_2 - \frac{1}{4}O_2 \tag{2}$$

$$\frac{1}{2}UO_2 + \frac{1}{2}PuO_{1.5} = U_{0.5}Pu_{0.5}O_2 - \frac{1}{8}O_2 \tag{3}$$

with which these endmembers could be formed from an equivalent mixture of UO_2 and $PuO_{1.5}$. These reactions involve a simultaneous annihilation of a certain amount of O_2 gas in the environment. The annihilation energy is equal to the negative of the chemical potential of O_2 times the amount of n moles of O_2 gas consumed. In our modelling approach, this energy is directly included into the definition of the free energy of an endmember i

$$G_i = \Delta G_i^0 - \left(T - T^0\right)\Delta S_i^0 + \Delta Cp_i^0\left(T - T^0 - Tln\left(\frac{T}{T^0}\right)\right) - \Delta n_i \mu_{O_2}^{T,P_{O2}} \tag{4}$$

where ΔG_i^0, ΔS_i^0 and ΔCp_i^0 are the changes in the standard state properties of oxides due to the reactions (1–3). The chemical potential of O_2 at a given temperature and at a given partial pressure is computed via the equation [10]:

$$\mu_{O_2}^{T,P_{O2}} = -S_{O_2}^0\left(T - T^0\right) + Cp_{O_2}^0\left(T - T^0 - Tln\left(\frac{T}{T^0}\right)\right) + RT\ln\left(P_{O_2}/P^0\right) \tag{5}$$

where $S_{O_2}^0 = 205.1373$ J/K/mol and $Cp_{O_2}^0 = 29.355$ J/K/mol and where P^0 is the standard pressure of 101325 Pa, $T^0 = 298.15K$. ΔG_i^0, ΔS_i^0 and ΔCp_i^0 in Eq. (1) are considered as fitting parameters.

The reference Gibbs free energy is modelled with the equation.

$$G^{ref} = \sum_i x_i G_i \tag{6}$$

The endmember fractions, x_i, are defined as follows. First, a completely reduced solid solution is built as a mixture of z moles of $PuO_{1.5}$ and $1-z$ moles of UO_2. Then, r moles of $PuO_{1.5}$ and r moles of UO_2 are allowed to react with each other forming $2r$ moles of $U_{0.5}Pu_{0.5}O_2$. Further, the remaining fractions $z–r$ of $PuO_{1.5}$ and $1–z–r$ of UO_2 are allowed to partially oxidize and form q moles of PuO_2 and x moles of $UO_{2.5}$, respectively. The final fractions of UO_2, $PuO_{1.5}$, PuO_2, $UO_{2.5}$ and $U_{0.5}Pu_{0.5}O_2$ become $1–z–r–x$, $z–r–q$, q, x and $2r$, respectively. In this notation, the non-stoichiometry parameter is computed as $\delta = 0.5(x-y)$, where $y = z–r–q$. The variables x, q and r determine the extent of reactions (1–3) and, thus, the oxidation state. Their equilibrium values are computed via the minimization of the total Gibbs free energy of mixing at a given temperature and a partial pressure of oxygen. Besides the reference energy, the total Gibbs free energy of mixing includes the excess free energy and the entropy of mixing. The excess free energy is modelled with the equation

$$G^{exess} = \sum\nolimits_{j \neq i} x_i x_j \left(W_{ij}^h - TW_{ij}^s\right) \tag{7}$$

where W_{ij}^h and W_{ij}^s are the enthalpic and entropic binary Margules parameters. The parameters relevant to the interaction between UO_2 and $UO_{2.5}$ and between $PuO_{1.5}$ and PuO_2 are determined by fitting to available phase equilibrium data. The other parameters are estimated based on the equation [11]:

$$W_{ij}^h = \frac{1}{6}\overline{EV}\left(\frac{V_i - V_j}{\overline{V}}\right)^2 \tag{8}$$

where V_i is the molar volume of an endmember i and where $\overline{E}$ and $\overline{V}$ are the average Young modulus and the average molar volume, respectively. The average Young modulus is taken to be 235 GPa (the average of the data for UO_2 and PuO_2 [12]).

The entropy of mixing is modelled with three equations. The first equation

$$S_M^{conf} = -t_0 R\left(t_1 \ln t_1 + t_2 \ln t_2 + t_3 \ln t_3 + t_4 \ln t_4\right) \tag{9}$$

with $t_0 = 1-x-y$, $t_1 = (1-z-r-x)/t_0$, $t_2 = q/t_0$, $t_3 = r/t_0$ and $t_4 = r/t_0$, describes the mixing of cations at the metal site. This equation implies that not all cations are allowed to be mixed with each other. Particularly, the amount x of U^{+5} cations and the amount y of Pu^{+3} cations, which are needed for charge balancing of oxygen interstitials and oxygen vacancies, respectively, are excluded from the mixing. The second equation

$$S_{Oi/Vi}^{conf} = -(R/3)\left(\left(\frac{3x}{2}\right)\ln\left(\frac{3x}{2}\right) + \left(1 - \frac{3x}{2}\right)\ln\left(1 - \frac{3x}{2}\right)\right) \tag{10}$$

models the entropy of mixing of interstitial oxygen anions and interstitial vacancies at the interstitial site. The O-interstitials are assumed to occupy a restricted sublattice within the interstitial site such that the total fraction of O-interstitials cannot exceed 1/3 [9]. The third equation

$$S_{O/V}^{conf} = -(2 - 1.5y)R((c)\ln(c) + (1 - c)\ln(1 - c)) \tag{11}$$

where $c = 0.5y/(2-1.5y)$, models the entropy of mixing between the vacancies and the lattice oxygen anions. This equation interpolates between the state of random mixing,

which is expected at a low fraction of vacancies, and a hypothetical ordered state, in which vacancies occupy one quarter of available oxygen sites. The latter state emulates the effect of repulsion between the vacancies at first and second near-neighbour distances. Consistently with this model, the $PuO_{1.5}$ endmember is assumed to have an ordered pyrochlore-type structure, $Pu_2Pu_2O_6VV$, in which vacancies, V, occupy a BCC sublattice within the oxygen lattice of fluorite.

Ion-packing model for the lattice parameter

The lattice parameter variation of doped UO_2 fluorite as functions of composition, non-stoichiometry, and type of a lanthanide dopant has been recently successfully modelled with the aid of an ion-packing model [9, 13]. This model uses the geometrical relationship between the lattice parameter, a, and the sum of the average radii of cations, $\langle R_C \rangle$, and anions,$\langle R_A \rangle$

$$a = \frac{4}{\sqrt{3}}\left(\langle R_C \rangle + \langle R_A \rangle\right) \tag{12}$$

Here, this model is applied to $U_{1-z}Pu_zO_{2+\delta}$. The average radii of cations and anions are evaluated as sums of radii of all cation and anion species weighted by their fractions in the structural formula $\{U^4_{1-z-r-x}U^5_rPu^3_{z-q}Pu^4_q\}U^{5*}_x\{O_{2-0.5y}V_{0.5y}\}Oi_{0.5x}$, where the upper indices denote cation charges. As the equilibrium fractions of cations and anions in this formula are functions of equilibrium fractions of the endmembers of the thermodynamic model, the lattice parameter is a function of the thermodynamic parameters of the equilibrium state. The cations taken in the curly brackets split into fractions of six-, seven- and eight-fold coordinated species. The latter are calculated under the approximation that vacancies occupy a BCC sublattice within the oxygen lattice of fluorite. As the fraction of vacancies in this sublattice is y, and as each cation is shared by two sites of the BCC sublattice, the fractions of six-, seven- and eight-fold species are y^2, $2y(1-y)$ and $(1-y)^2$, respectively. For example, the fraction of U^{+4} in eight-fold coordination (shortly $U^{4,8}$) is computed as $(1-z-r-x)(1-y)^2$. The U^{5*} cations that are not included in the curly brackets are assumed to have one or two interstitial O^{-2} anions in their close neighbourhood. Following the study of Vinograd et al. [9], the U^{5*} cations are assigned a radius that is smaller than the radius of U^{+5} in eight-fold coordination. This is done to emulate the effect of the lattice contraction caused by O-interstitials. The average radius of an anion is composed only from the contributions of the lattice oxygen and the oxygen vacancy. The effective size of the vacancy is taken to be substantially larger than the ionic radius of lattice oxygen, as discussed in previous studies [9, 13, 14]. It should be noted that the developed ion-packing model can be also applied for the calculation of volumes of the endmembers ($V_i = a_i^3$) and, consequently, for the estimation of Margules binary interaction parameters via Eq. (8).

Results

Determination of thermodynamic parameters

The standard properties of the $UO_{2.5}$ endmember are adopted from the study of Vinograd et al. [9]. The standard properties of PuO_2 are determined here by fitting to high-temperature data describing the dependence of the non-stoichiometry parameter δ in $(Pu^4_{1-y}Pu_y^3)O_{2-0.5y}$ on the chemical potential of O_2 [15–18]. This fitting also includes the adjustment of the Margules parameters in the binary $PuO_{1.5}$–PuO_2. The fitted parameters are given in Table S1 (Supplementary Materials); the predicted isotherms are shown in Fig. 1. The fitted standard Gibbs free energy and entropy parameters of PuO_2 ($\Delta G^0_{PuO2} = -215.6$ kJ/mol and $\Delta S^0_{PuO2} = -15.4$ J/K/mol) are in a reasonable agreement with the corresponding differences in the standard properties of PuO_2 and ½ Pu_2O_3 given in the review study of Chartier et al. [19]. The enthalpic W^h parameter of 54.0 kJ/mol appears to be significantly larger than the value of ~ 5.8 kJ/mol, which is estimated from the volume-difference relationship (Eq. 8). A similar level of disagreement is observed between the fitted and computed enthalpic Margules parameters for the UO_2–$UO_{2.5}$ binary (29.0 kJ/mol (fitted) [9] vs. 0.9 kJ/mol (estimated with Eq. 8)). The likely reason for the disagreement is that in the cases of $PuO_{1.5}$–PuO_2 and UO_2–$UO_{2.5}$ the Margules parameters reflect not only the elasticity effects, but also effects of a nonlinear variation of the Gibbs free energy with the extent of the oxidation, i.e. with the δ parameter. The large positive W^h parameter determined in the $PuO_{1.5}$–PuO_2 binary is primarily responsible for the miscibility gap in the UO_2–$PuO_{1.5}$–PuO_2 system below 1000 K. Consequently, the values of W^h and W^s are adjusted such that both the data on ΔG_{O_2} vs. δ (Fig. 1) and the data on the composition of the exsolved phases (Fig. 2) are fitted equally well. The phase separation is modelled by allowing the two phases to have different y parameters, but the same z parameter (see Supplementary Materials). This is consistent with the assumption that the phase separation is made possible due to the fast diffusion of oxygen and by an instantaneous oxidation/reduction of Pu and U cations.

The standard properties of the $U_{0.5}Pu_{0.5}O_2$ endmember, in principle, could be fitted to available δ vs. ΔG_{O_2} data on $(U_{1-z}Pu_z)O_{2+\delta}$ samples with z varying in the range $0.12 < z < 0.4$. An attempt to do this was, however, unsuccessful. The best fit was achieved with a positive value of $\Delta G^0_{U0.5Pu0.5O2}$, which made the fraction the $U_{0.5}Pu_{0.5}O_2$ endmember effectively zero. Therefore, we assume this endmember to be redundant. Apparently, it loses competition with an equal mixture of UO_2 and PuO_2 endmembers. In the calculations $\Delta G^0_{U0.5Pu0.5O2}$ was set arbitrarily to 100 kJ/mol.

Determination of parameters of the ion-packing model

The radii of O^{-2} and the radii of U^{+4} and U^{+5} in six-, seven- and eight-fold coordination are adopted from the study of Vinograd et al. [9]. The radii of Pu^{+3} and Pu^{+4} are evaluated here via fitting to lattice parameter data on Pu-doped UO_2 [4, 5, 24]. The radius of $Pu^{4,8}$ of 0.963 Å is adjusted to the lattice parameter data of Markin & Street [4] for stoichiometric, $(U_{1-z}Pu_z)O_2$, samples. The radius of $Pu^{4,6}$ of 0.86 Å is taken from Shannon [25] and the radius of $Pu^{4,7}$ of 0.9115 Å is set equal to the average of the radii of $Pu^{4,6}$ and $Pu^{4,8}$. The radius of $Pu^{3,6}$ of 1.0 Å is taken from Shannon [25] and the vacancy radius of 1.465 Å is fixed by fitting to the data of Benedict et al. [24] on completely reduced samples, $(U_{1-z}Pu_z)O_{2-z/2}$. The radius of $Pu^{3,8}$ is adjusted to the value of 1.12 Å following a correlation between the radii of $M^{3,8}$ and $M^{3,6}$ for M = *Ln* [14] and then tuned to a slightly lower value of 1.11 Å according to the data plotted in Figs. 3 and 4. The radius of $Pu^{3,7}$ of 1.055 Å is taken to be the average of the radii of $Pu^{3,6}$ and $Pu^{3,8}$. The radii are given in Table S2 (Supplementary Materials).

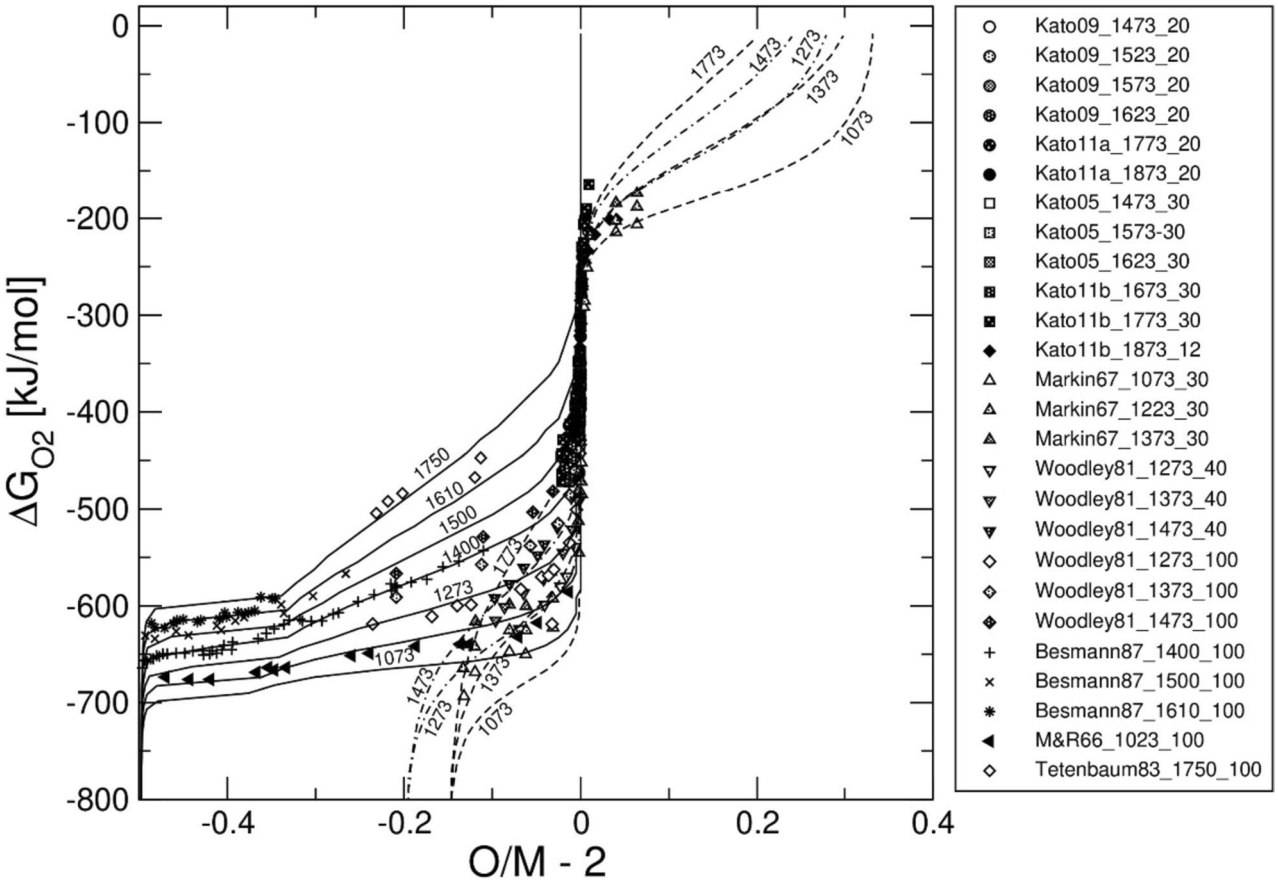

Fig. 1 Model fit to the experimental data on ΔG_{O_2} vs. δ ($\Delta G_{O_2} = RT\ln(P_{O_2}/P^0)$, $\delta = O/M - 2$) in $U_{1-z}Pu_zO_{2+\delta}$. The experimental data are from Markin and Mc Iver [20], Woodley [16], Besmann [18], Markin and Rand [15], Tetenbaum [17] and Kato et al. (see Supplementary Materials for the legend notations and references). Solid, dashed-dotted and dashed isotherms correspond to $z = 1.0$, $z = 0.4$ and $z = 0.3$, respectively. The breaks in the $z = 1.0$ isotherms at low O/M values are modelled as a two-phase equilibrium of fluorite with a phase of $PuO_{1.5}$ composition. The fitted standard Gibbs free energy and the entropy of this phase are 5.0 kJ/mol and 9.7 J/K/mol, respectively

The ion-packing model upon the combination with the thermodynamic model allows mapping the gap isotherms on a diagram that plots the lattice parameter measured at room temperature against the Pu/(Pu + U) ratio (Fig. 3). A combination of the lattice parameter model with the thermal expansion equation of Martin [29] allows plotting the lattice parameters of exsolved phases as functions of the temperature simulating an in situ X-ray diffraction experiment (Fig. 4).

Discussion and conclusion

The developed model provides a consistent description of the thermodynamic and structural data. ΔG_{O_2} isotherms in Fig. 1 pass through most of the datasets, except for the data obtained in the lowest temperature range (1023 K, $z = 1.0$ and 1073 K, $z = 0.3$) of Markin and Rand [15] and Markin and Mc Iver [20], respectively. We also had difficulties in fitting the data of Sari et al. [5] for Pu-rich samples ($z = 0.8$) (Fig. 2). The gap closing temperature of ~ 1000 K predicted here is in a good agreement with the thermodynamic assessment study of Guéneau et al. [8]. The data of Sari et al. [5] and the data of Truphémus et al. [26] referring to the lattice parameters of two co-existing fluorite phases (Fig. 3) are fitted well assuming the closing temperature of O-diffusion between 373 and 473 K. The data of Vaudez et al. [27] and Vigier et al. [28] suggest a partial non-equilibrium oxidation of the low-oxygen phase. A possible explanation is that the oxygen diffusion is significantly faster in the low-oxygen phase at ambient temperatures such that there is an experimental difficulty in quenching the oxygen partitioning between the two phases. A very good agreement is achieved with the data of Markin & Street [4] and with the data of Belin et al. [30] measured in situ (Fig. 4). The diagram is consistent with the assumption that certain low-oxygen samples of Belin et al. [30] experienced a partial non-equilibrium oxidation during cooling runs, as discussed by Belin et al. [30].

The fitted cation radii of Pu^{+3} and Pu^{+4} are in a good agreement with values tabulated by Shannon [29]. The effective radius of a vacancy of 1.465 Å is, however,

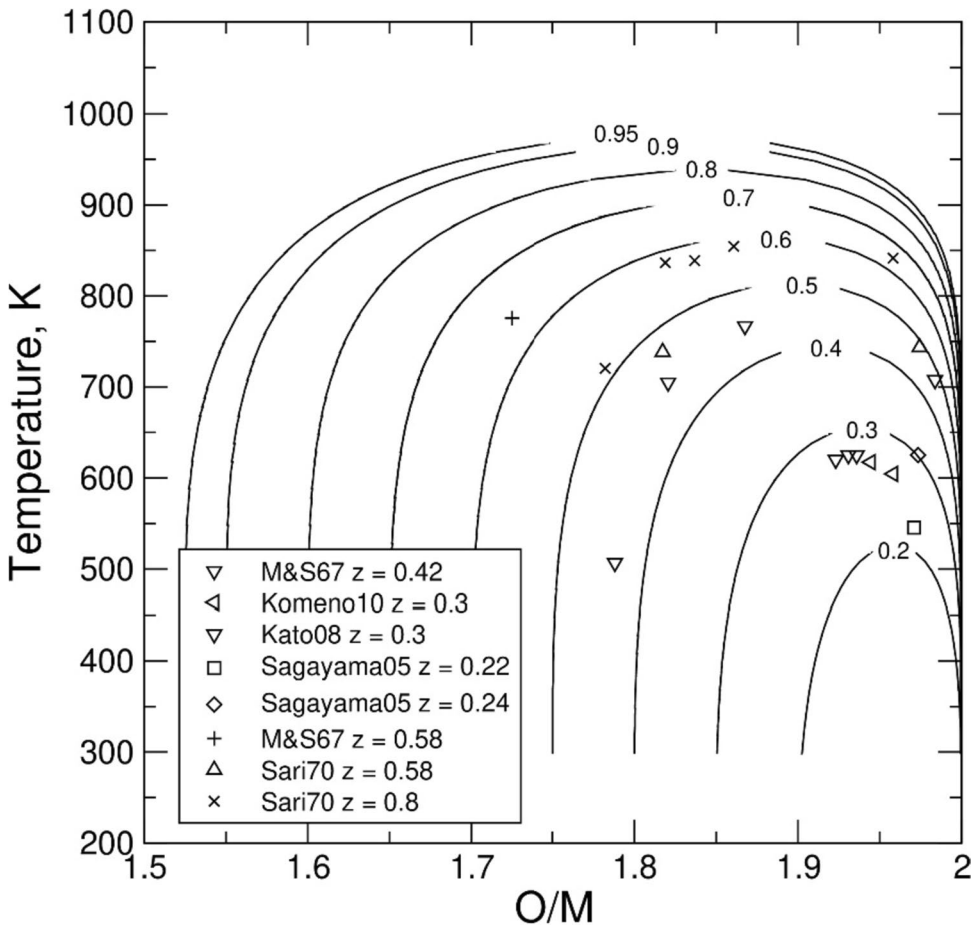

Fig. 2 The O/M values of the co-existing fluorite phases with Pu/(Pu + U) ratios plotted as functions of the temperature. The experimental data are from Markin and Street [4], Komeno et al. [21], Kato et al. [22], Sagayama [23] and Sari et al. [5]

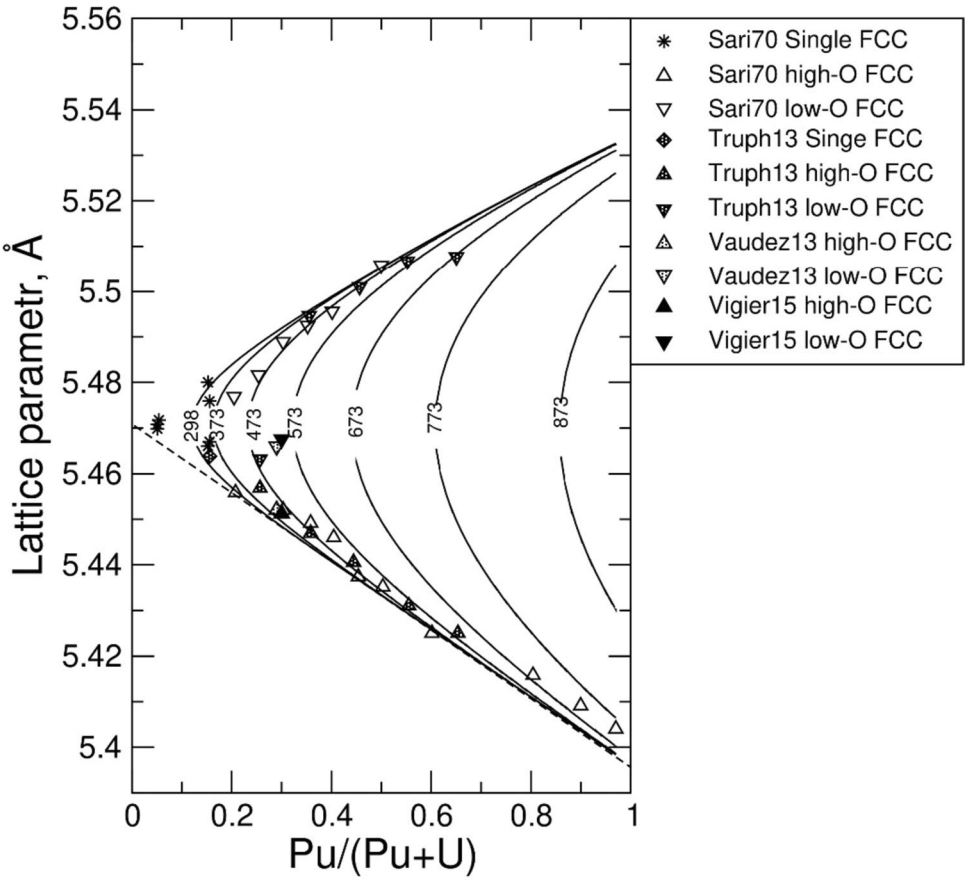

Fig. 3 Lattice parameters of exsolved FCC phases plotted against the composition variable. The solid lines denote the predicted isotherms. The experimental data are from Sari et al. [5], Truphémus et al. [26], Vaudez et al. [27] and Vigier et al. [28]. The dotted line corresponds to the strictly stoichiometric state

smaller than that used in the study of lanthanide-doped UO_2 [9]. This observation suggests that the size of a vacancy might not be transferrable from lanthanide-doped to Pu-doped UO_2.

An interesting result is the redundancy of the $U_{0.5}Pu_{0.5}O_2$ endmember. A similar endmember with the composition of $U_{0.5}Ln_{0.5}O_2$ was found to be very important in the study of lanthanide-doped UO_2 [9]. This redundancy suggests that the substitution mechanism of $2U^{+4} = U^{+5} + Pu^{+3}$ is ineffective in Pu-doped UO_2. A possible implication is that $U^{+5} + Pu^{+3}$ react to $U^{+4} + Pu^{+4}$, and, consequently, U^{+5} and Pu^{+3} should not occur in stoichiometric Pu-doped UO_2. In Ln-doped UO_2 the situation is different because an analogous reaction is not possible due to the instability of Ln^{+4}. This hypothesis should be tested by spectroscopic methods.

The computed diagrams provide a frame of reference that could help in the detection of phase separation and of partial oxidation in hypo-stoichiometric samples synthesized or quenched at the thermodynamic parameters of the miscibility gap.

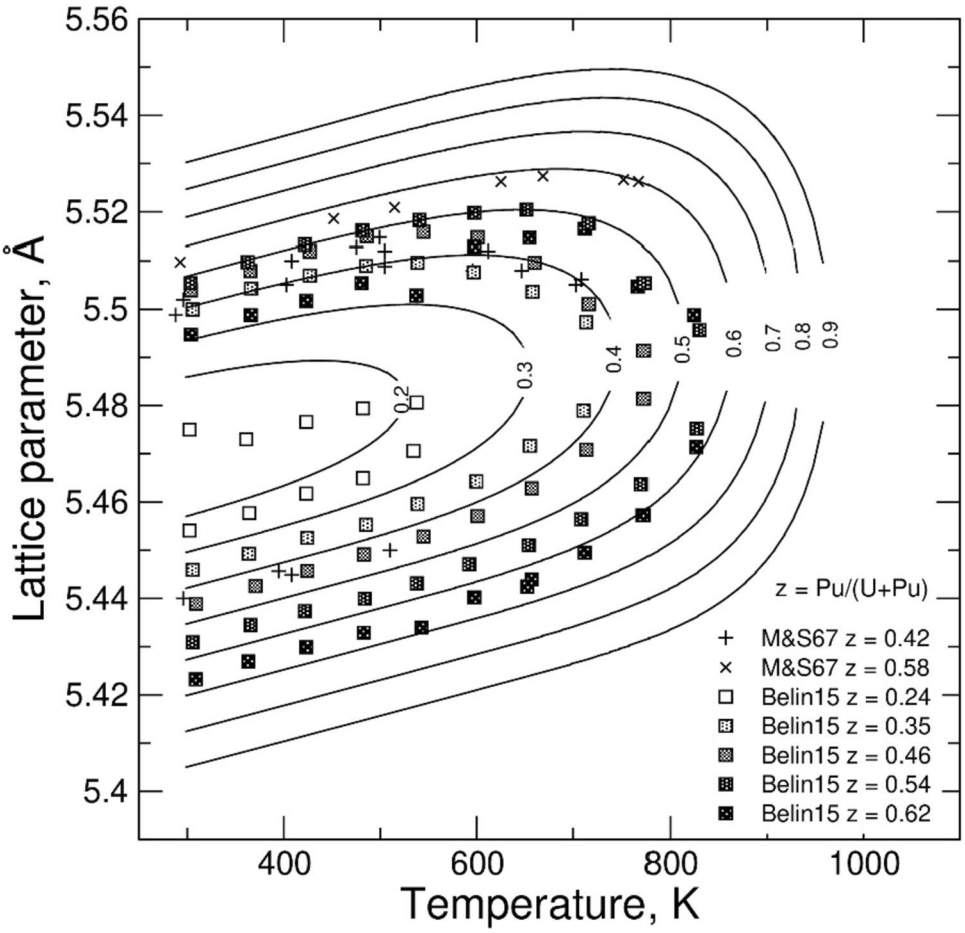

Fig. 4 Lattice parameters of exsolved FCC phases plotted against the temperature. The lines denote fixed sample compositions. The experimental data are from Markin & Street [4] and Belin et al. [30]. The diagram is constructed using the thermal expansion equation of Martin [29] for the interval $273\ K < T < 923\ K$

Supplementary Information The online version contains supplementary material available at https://doi.org/10.1557/s43580-024-00818-z.

Author contributions V.L.V. developed the thermodynamic model, performed the calculations, and wrote the text. A.A.B. contributed to structure-relevant aspects of the model and to analysis of the results. G.M. and G.D. contributed to conceptualization, to discussion of the results, and helped to shape the manuscript.

Funding Open Access funding enabled and organized by Projekt DEAL. Not applicable.

Data availability The datasets generated during and/or analyzed during the current study are available from the corresponding author on reasonable request.

Declarations

Conflict of interest There are no conflicts to declare.

References

1. C. Douglas, D.C. Crawford, D.L. Porter, S.L. Hayes, J. Nucl. Mater. **371**, 202 (2007)
2. M. Odorowski, Ch. Jégou, L. De Windt, V. Broudic, S. Peuget, M. Magnin, M. Tribet, Ch. Martin, J. Nucl. Mater. **468**, 17 (2016)

3. V. Kerleguer, C. Jégou, L. De Windt, V. Broudic, G. Jouan, S. Miro, F. Tocino, C. Martin, J. Nucl. Mater. **529**, 151920 (2020). https://doi.org/10.1016/j.jnucmat.2019.151920
4. T.L. Markin, R.S. Street, J. Inorg. Nucl. Chem. **29**, 2265 (1967)
5. C. Sari, U. Benedict, H. Blank, J. Nucl. Mater. **35**, 267 (1970)
6. T.M. Besmann, T.B. Lindemer, J. Nucl. Mater. **130**, 489 (1985)
7. Ch. Guéneau, Ch. Chatillon, B. Sundman, B., J. Nucl. Mater. **378**, 257 (2008)
8. C. Guéneau, N. Dupin, B. Sundman, C. Martial, J.C. Dumas, S. Gossé, S. Chatain, F. De Bruycker, D. Manara, R.J. Konings, J. Nucl. Mater. **419**(1–3), 145–167 (2011)
9. V.L. Vinograd, A.A. Bukaemskiy, G. Deissmann, G. Modolo, Sci. Rep. **13**, 17944 (2023)
10. M.V. Finnis, A.Y. Lozovoi, A. Alavi, Ann. Rev. Mater. Res. **35**, 167 (2005). https://doi.org/10.1146/annurev.matsci.35.101503.091652
11. P.M. Kowalski, Y. Li, J. Europ. Ceram. Soc. **36**, 2093 (2016)
12. M. Kato, T. Matsumoto, Thermal and Mechanical Properties of UO_2 and PuO_2. (NEA/NSC/R(2015)2, 172, 2015) https://inis.iaea.org/collection/NCLCollectionStore/_Public/47/093/47093736.pdf
13. V.L. Vinograd, A.A. Bukaemskiy, G. Modolo, G. Deissmann, D. Bosbach, Front. Chem. **9**, 705024 (2021). https://doi.org/10.3389/fchem.2021.705024
14. A.A. Bukaemskiy, V.L. Vinograd, P.M. Kowalski, Acta Mater. **202**, 99 (2021). https://doi.org/10.1016/j.actamat.2020.10.045
15. T.L. Markin, M.H. Rand, in Thermodynamics, vol. 1, Proceedings of the Symposium held in Vienna, 22–27 July 1965 (IAEA, Vienna, 1966), p. 145.
16. R.E. Woodley, J. Nucl. Mater. **96**, 5 (1981)
17. M. Tetenbaum, in Plutonium Chemistry, Am. Chem. Soc. Symp. Ser. 216, (Am. Chem. Soc., Washington, 1983), p. 109.
18. T.M. Besmann, J. Nucl. Mater. **144**, 141 (1987)
19. A. Chartier, L. Van Brutzel, P. Fossati, Ph. Martin, C. Guéneau, *Comprehensive Nuclear Materials* (Elsevier, Amsterdam, 2020)
20. T.L. Markin, E.J. Mc Iver, in Plutonium 1965, Proc. 3rd Int. Conf. on Plutonium, London, 1965, (Chapman and Hall, London, 1967), p.845.
21. A. Komeno, M. Kato, H. Uno, K. Takeuchi, K. Morimoto, M. Kashimura, in Actinides 2009, IOP Conf. Series: Materials Science and Engineering, vol. 9, (2010), p. 012016
22. M. Kato, K. Morimoto, H. Sugata, K. Konashi, M. Kashimura, T. Abe, J. Nucl. Mater. **373**, 237 (2008)
23. Y. Sagayama, in: Global 2005, Proceedings of the international conference on nuclear energy systems for future generation and global sustainability, October 9–13, Tsukuba, Japan, (2005), Paper 380.
24. U. Benedict, M. Coquerelle, J. De Bueger, C. Dufour, J. Nucl. Mater. **45**, 217 (1972)
25. R. Shannon, Acta Cryst. **A32**, 751 (1976). https://doi.org/10.1107/S0567739476001551
26. T. Truphémus, R.C. Belin, J.C. Richaud, M. Reynaud, M.A. Martinez, I. Félines, A. Arredondo, A. Miard, T. Dubois, F. Adenot, J. Rogez, J. Nucl. Mater. **432**, 378 (2013)
27. S. Vaudez, R.C. Belin, L. Aufore, P. Sornay, S. Grandjean, J. Nucl. Mater. **442**, 227 (2013)
28. J.-F. Vigier, M. Philippe, Ph.M. Martin, L. Martel, D. Prieur, A.C. Scheinost, J. Somers, Inorg. Chem. **54**, 5358 (2015)
29. D.G. Martin, J. Nucl. Mater. **152**, 94 (1988)
30. R.C. Belin, M. Strach, Th. Truphémus, Ch. Guéneau, J-Ch. Richaud, J. Rogez, 2015 Adag. J Nucl Mater 465: 407